OXFORD

SOT | Society of Toxicology
www.toxsci.oxfordjournals.org

TOXICOLOGICAL SCIENCES, 153(1), 2016, 4–17

doi: 10.1093/toxsci/kfw101
Advance Access Publication Date: June 2, 2016
Research article

Abrasion of Artificial Stones as a New Cause of an Ancient Disease. Physicochemical Features and Cellular Responses

Cristina Pavan,[*,‡,1] Manuela Polimeni,[†,‡,1] Maura Tomatis,[*,‡,2] Ingrid Corazzari,[*,‡] Francesco Turci,[*,‡] Dario Ghigo,[†,‡,3] and Bice Fubini[*,‡]

[*]Department of Chemistry, University of Torino, Turin 10125, Italy, [†]Department of Oncology, University of Torino, Turin 10126, Italy and [‡] "G. Scansetti" Interdepartmental Center for Studies on Asbestos and Other Toxic Particulates, University of Torino, Turin 10125, Italy

[1]These authors contributed equally to this study.

[2]To whom correspondence should be addressed at Department of Chemistry, University of Torino, Via P. Giuria 7, 10125 Turin, Italy. Fax: +39 0116707855. E-mail: m.tomatis@unito.it

[3]Professor Dario Ghigo passed away on October 7, 2015. He was not only a wonderful teacher and colleague but also a dear friend. He represented an uncommon example of correctness, honesty, and integrity. Dario will be always with us.

ABSTRACT

New outbursts of silicosis were recently reported among workers manufacturing an engineered material known as "artificial stone," composed by high percentages of quartz (up to 98%) agglomerated with pigments and polymeric resins. Dusts released by abrasion during artificial stone polishing were characterized for particle size, morphology, and elemental composition and studied for (1) ability to catalyze free radical generation in acellular tests, (2) membranolytic potential on human erythrocytes, (3) cytotoxic activity (lactate dehydrogenase release) on murine alveolar macrophages (MH-S) and human bronchial epithelial (BEAS-2B) cell lines, (4) induction of epithelial-mesenchymal transition (EMT) in BEAS-2B cells. Min-U-Sil 5 was used as reference quartz. Artificial stone dusts exhibited morphological features close to quartz, but contained larger amount of metal transition ions (mainly, Fe, Cu, and Ti), potentially responsible for the high reactivity in free radical generation observed. Opposite to Min-U-Sil 5, they were neither hemolytic nor cytotoxic on MH-S cells, a low cytotoxicity only being observed with BEAS-2B cells. The presence on the particle surface of residues of the resin accounts for this attenuated behavior, as hemolysis appeared and cytotoxicity increased after thermal degradation of the resin, when the free quartz surface was exposed. All dusts induced EMT with loss of E-cadherin expression and increased the expression of mesenchymal proteins (α-smooth muscle actin and vimentin). This may contribute to explain the development of fibrosis on workers exposed to artificial stone dusts.

Key words: quartz; artificial stone; free radical; membranolysis; cytotoxicity; epithelial–mesenchymal transition

Occupational exposure to dusts produced during manufacturing of "artificial stones," also known as "quartz conglomerates," was associated with an increased incidence of silicosis, one of the most ancient occupational diseases (Sauvé, 2015; Steenland and Ward, 2014). Several clusters of silicosis and lung-associated pathologies such as autoimmune diseases (Shtraichman *et al.*, 2015) were reported in the past few years due to fabrication and installation of artificial stones used primarily for kitchen and bathroom countertops in Spain (García Vadillo *et al.*, 2011; Martínez *et al.*, 2010; Pascual *et al.*, 2011; Pérez-Alonso *et al.*, 2014), Israel (Kramer *et al.*, 2012), Italy (Bartoli *et al.*, 2012), and in the United States (Bang *et al.*, 2015; Friedman *et al.*, 2015). Moreover, a recent hazard alert for workers manufacturing, finishing and installing countertops was

issued by the Occupational Safety and Health Administration and the Center for Disease Control and Prevention (NIOSH, 2015).

Concern for workers' health derives from the high crystalline silica content in artificial stones, which are blends of quartz (even over 90%) with pigments and polymeric resins providing the characteristic strength, water resistance, and color variety. Thus, during various steps in the manufacturing procedure (cutting, grinding, chipping, sanding, drilling, and polishing), workers may be exposed to respirable (aerodynamic diameter < 5 μm) crystalline silica dusts known to cause silicosis, lung cancer, or obstructive pulmonary disease, which may progress to respiratory failure and death (International Agency for Research on Cancer (IARC), 2012). Despite efforts to prevent crystalline silica exposure, all silicosis cases associated to artificial stone processing are related to a lack of preventive measures such as particulate abatement systems or personal respiratory protections. Thus, the large amount of dusts inhaled in a short period of time may, in part, explain the strikingly short-latency and the severity of the observed disease. Indeed, most epidemiological and clinical reports associated to artificial quartz conglomerates described cases of accelerated silicosis occurring within a few years of exposure and even affecting young subjects (Paolucci *et al.*, 2015; Pérez-Alonso *et al.*, 2015). Nevertheless—as proposed by Paolucci *et al.* (2015)—the extent of the damage suggests that besides high exposure levels, the chemical characteristics of the inhaled particles should also be taken into account, as dusts generated by cutting artificial conglomerates contain not only silica but also resins and pigments that may modify silica reactivity.

In this view, the aim of the present research was to explore the physicochemical properties and the *in vitro* biological reactivity that could be relevant for the reported high pathogenicity of artificial stone dusts. Size, morphology, chemical composition, and surface reactivity of the dusts were thoroughly evaluated. In particular, we investigated the generation of free radicals—a process known to contribute to the overall toxicity (Fubini and Hubbard, 2003)—in acellular systems, and membranolytic potential on human red blood cells (RBCs). Despite RBCs play no a direct role in the pathogenesis of silicosis or lung cancer, RBC membrane is a simple and convenient model to investigate damage to biological membranes, which represent one of the first sites of interaction with particulate matter. Moreover, the hemolysis test is one of the best predictive tests of particle-induced inflammatory response (Cho *et al.*, 2013; Lu *et al.*, 2009; Pavan *et al.*, 2014). Recent studies have shown that silica particles can induce the release of proinflammatory cytokines (eg, interleukin-1β) via a membranolytic mechanism involving phagolysosomal membrane destabilization (Hornung *et al.*, 2008; Hughes *et al.*, 2016) and a correlation between the hemolytic activity of a set of silica particles, and release of IL-1β from macrophages was observed (Pavan *et al.*, 2014). Cell toxicity was evaluated *in vitro* on human bronchial epithelial (BEAS-2B) cells, as well as on murine alveolar macrophages (MH-S), and the occurrence of the epithelial-mesenchymal transition (EMT) in BEAS-2B cells was also investigated. Fibrosis is a multiorigin disease but EMT has been recently recognized as an important pathway in cell transformation (Blanco *et al.*, 2004; Li and Li, 2015; Nowrin *et al.*, 2014) and in particulate-induced lung fibrosis such as silicosis (Hu Yong *et al.*, 2015; Liang *et al.*, 2015; Rong *et al.*, 2015).

The artificial stone dusts here considered were obtained by 2 types of processing—dry and wet—and were collected in different Italian companies where some cases of silicosis had been reported (Bartoli *et al.*, 2012). The study was performed by comparing the physicochemical properties and the cellular effects of artificial stone dusts with those of a largely used reference quartz (Min-U-Sil 5) known for its cytotoxic and fibrogenic activity (International Agency for Research on Cancer (IARC), 1997).

MATERIALS AND METHODS

Materials

Artificial stone dust samples

A set of samples kindly supplied by the USL 11 of Empoli (FI, Italy) was collected in several Italian companies specialized in the manufacturing of quartz conglomerates. The samples consisted of dusts deposited *in situ* following 2 types of processing of the same material: a dry cutting (dry) using a grinding machine and a wet cutting (wet) using a circular saw or pantograph followed by water abatement to reduce airborne particles. All samples were examined for their chemical composition and oxidative activity in cell-free tests. Particle size, morphology, and cellular responses were performed on samples 1 and 2 (dry and wet), identified as the most reactive in generating free radicals. We report here the main results obtained on samples 1 and 2. The results obtained for samples 3, 4, 5, 6, and 7 are reported in the Supplementary data. One further sample (8-dry) was provided by the ASL 19 of Asti (AT, Italy) in the form of brick. A respirable dust was obtained by dry cutting of the brick using a diamond grinding wheel. The dust was tested 3 hours and 2, 8, and 15 days after preparation to evaluate the effect of aging on free radical release. Origins and acronyms of the samples dealt with in the text are listed in Table 1.

Reference quartz

The commercial quartz Min-U-Sil 5 purchased from U.S. Silica Co (Berkeley Springs, West Virginia; lot number 15062696) was used as positive control. Qz(Min-U-Sil 5) physicochemical features have been previously described by some of us (Gazzano *et al.*, 2012; Ghiazza *et al.*, 2013; Pavan *et al.*, 2013). A synthetic amorphous silica (MSS) from Fiber Optic Center Inc (New Bedford, Massachusetts) was used as negative control in EMT experiments. It is made up of regular monodispersed silica spheres ranging around 1 μm in diameter. It was characterized and found inert in previous *in vitro* studies (Gazzano *et al.*, 2012; Ghiazza *et al.*, 2010).

Chemical reagents

When not otherwise specified, all reagents were purchased from Sigma-Aldrich (Milan, Italy). The water used was ultrapure Milli-Q water (Millipore, Billerica, Massachusetts), and 5,5'-dimethyl-1-pirroline-N-oxide (DMPO) was purchased from Cayman Chemical Company (Ann Arbor, Michigan).

Physicochemical Treatments of the Dusts

Heating of artificial stone dusts. Three grams of the dusts obtained either by dry and wet processing of sample 1 were heated in air at 500°C for 1 hour in order to promote degradation of the polymeric resin present in those samples. The samples thermally treated are indicated as 1-wet(h) and 1-dry(h).

Grinding of artificial stone dusts. Part of the dusts obtained either by dry and wet processing of sample 1 and previously heated in air at 500°C was further ground in a mixer mill (27 Hz) in agate jars (500 mg of sample per jar) for 1 hour in order to simulate the abrasion of the material at the time of processing. The samples

TABLE 1. List and Source of the Artificial Stone Dusts Studied

Pristine Samples	Sampling Site/Origin	Treated Samples	Treatment
1-wet	Circular saw- water abatement	1-wet(h) 1-wet(h/g)	Heated at 500 °C in air; heated/ground in a mixer mill for 1 hour
1-dry	Dry grinding (grinding machine)	1-dry(h) 1-dry(h/g)	Heated at 500 °C in air; heated/ground in a mixer mill for 1 hour
2-wet	Circular saw-water abatement		
2-dry	Dry grinding (grinding machine)		
8-dry	Laboratory ground (diamond wheel)		
Qz(Min-U-Sil 5)	Commercial (ground mineral)		

first heated and then ground are referred to as 1-wet(h/g) and 1-dry(h/g).

Physicochemical Characterization

Morphological investigation. Sample morphology was studied by Scanning Electron Microscope (SEM) in the secondary electron image mode using a Zeiss EVO 50 XVP (Oberkochen, Germany) with LaB_6 source. The samples were dispersed in ultrapure water (at 0.5 mg/ml), sonicated for 2 minutes in ice with an ultrasonic probe (40 W; Sonoplus, Bandelin, Berlin, Germany), dropped off on conductive stubs and coated with gold. The operating conditions were as follows: EHT 15–25 kV, WD 1–6 mm, and probe current 50–40 pA.

Size analysis. Particle size distribution was obtained by flow particle image analysis using the Sysmex FPIA-3000 apparatus (Malvern Instruments, UK, detection range, 0.8–300 μm). This instrument measures the diameter of a circle having the same projected area of the particle image optically detected (ie, the circle equivalent or CE diameter). Artificial stone dusts were dispersed in ultrapure water (0.5 mg/ml) and sonicated for 30 seconds at 10 W. Each sample was run at least 4 times with objective lens at ×20 magnification in high-power field mode. The 4 analyses were then pooled to obtain a statistically sound size distribution.

Specific surface area. The specific surface area was measured by means of the BET method based on N_2 or Kr adsorption (depending on the surface area expected) at -196°C (ASAP 2020, Micromeritics, Norcross). Quartz samples have been degassed at 30°C for hours prior to N_2 or Kr analysis.

Elemental composition. Elemental composition was assessed by micro-X-ray florescence spectroscopy (μ-XRF) using an Eagle III-XPL spectrometer equipped with a Rh X-ray tube, an EDS Si(Li) detector and an Edax Vision32 microanalytical system. The dusts were pressed into thin self-supporting pellet and each sample was analyzed in 12 different points, each point being collected choosing 30 kV and 250 μA as, respectively, the voltage and the current of the X-ray tube and 17 μs as integration time.

Free radical detection. The potential to generate hydroxyl (HO) radicals from hydrogen peroxide (Fenton Activity) and carboxyl (COO^-) radicals from sodium formate (representative of the homolytic cleavage of C-H bonds in biomolecules) was investigated by Electron Paramagnetic Resonance (EPR) spectroscopy (Miniscope MS100; Magnettech, Berlin, Germany) coupled with the spin trapping technique. 5,5'-Dimethyl-1-pirroline-N-oxide (DMPO) was used as trapping agent following a well-established procedure (Fenoglio *et al.*, 2000; Fubini *et al.*, 1995b). The spectra were recorded at 10, 30, and 60 minutes after particle incubation.

Thermogravimetric analysis coupled with Fourier Transform Infrared Spectroscopy and Gas Chromatography Mass Spectrometry techniques. The nature and the amount of the residual volatiles evolved during the thermal analysis of artificial stone dusts were evaluated by means of an ultra-microbalance (sensitivity 0.1 μg) connected with a time-resolved Fourier Transform Infrared Spectroscopy (FTIR) detector. Thermal analyses were performed under oxygen or nitrogen atmosphere. Under oxygen atmosphere (flow rate: 35 ml/minute), the dusts (ca. 10 mg) were heated from 30°C to 600°C at the rate of 20°C/minute in a Pyris 1 Thermogravimetric (TGA) from Perkin-Elmer (Waltham, Massachusetts), whereas under nitrogen atmosphere (flow rate: 35 ml/minutes), the dusts were heated from 30°C to 900°C. The gas evolved during the heating ramp was piped (gas flow: 65 ml/min) via pressurized heated transfer line (Redshift S.r.l., Vicenza, Italy) and analyzed continuously by an FTIR spectrophotometer (Spectrum 100; Perkin-Elmer), equipped with a thermostated conventional gas cell. Temperature/time-resolved spectra were acquired in the 600–4000 cm^{-1} wavenumber range with a resolution of 0.4 cm^{-1} and analyzed with the Spectrum software (Perkin-Elmer). At the temperature where the main weight loss process reached the highest speed (ie, 450 °C) under N_2 atmosphere, the evolved gas (ca. 100 μl) was automatically pumped into a gas chromatograph (Clarus 500S; Perkin-Elmer) equipped with a standard nonpolar fused silica capillary column (Elite 5MS; Perkin-Elmer). Identification of the species contained in the eluate was performed with an integrated mass spectrometer (Clarus 560S; Perkin-Elmer). The results were reported as total ion count chromatograms, and the analysis of the average mass spectra at the chromatographic peak middle height was performed with the NIST MS Search Software.

In Vitro *Cell Tests*

Hemolysis assay on human erythrocytes. Erythrocytes were purified from fresh human blood obtained by healthy volunteer donors not receiving any pharmacological treatment. The method refers to Lu *et al.* (2009) with minor modifications given in Pavan *et al.* (2013). Briefly, erythrocytes were purified from blood collected in vacutainer tubes containing K_2EDTA as anticoagulant by centrifugation at 1200 × g for 10 minutes (Heraeus, Megafuge 11R; Thermo Scientific), they were washed 4 times with 0.9% NaCl (Eurospital S.p.a., Trieste, Italy), and finally suspended in 0.9% NaCl at the final concentration of 5% by volume. The dust samples were dispersed at the concentration of 200 cm^2/ml in 0.9% NaCl and sonicated during 2 minutes (40 W, Sonoplus HD 2070; Bandelin, Berlin, Germany). Serial dilutions of the starting dispersion were performed to the final concentrations used for experiments (200, 100, 50, 25, 12.5, and 6.25 cm^2/ml). Because RBC membranolysis is a surface-driven process, concentrations were calculated on the basis of the BET surface area for each sample. Particle suspensions were distributed in quadruplicate

in a 96-well plate (150 μl/well), and the RBC suspension was then added (75 μl/well). Negative and positive controls consisted in 0.9% NaCl and 0.1% Triton-X 100, respectively. The plate was incubated at room temperature on an orbital plate shaker for 30 minutes and then centrifuged at 1200 rpm for 5 minutes (Heraeus, Megafuge 1.0R; Thermo Scientific). Supernatants were finally transferred to a new plate (75 μl/well), and the absorbance of the hemoglobin released was determined at a wavelength of 540 nm on a microplate reader (Benchmark Plus, Bio-Rad, Hercules).

Cell cultures. Human bronchial epithelial cells (BEAS-2B; American Type Culture Collection, ATCC, Manassas, Virginia) and murine alveolar macrophages (MH-S, a continuous cell line derived from Balb/cJ mice; Istituto Zooprofilattico Sperimentale "Bruno Ubertini," Brescia, Italy) were cultured in Petri dishes in RPMI-1640 medium (Gibco, Paisley, UK) supplemented with 10% of fetal bovine serum and 1% penicillin (100 U/ml)—streptomycin (100 μg/ml) at 37°C in a 5% CO_2 humidified atmosphere.

Particle exposure. Particles were heated at 200°C for 2 hours in order to sterilize them and inactivate any trace of endotoxin, and then suspended in complete cell culture medium just before use and sonicated during 2 minutes (40 W, Sonoplus HD 2070). Cells were incubated with complete cell culture medium alone (negative control) or with different concentrations of the dusts, expressed as μg of dust per cm^2 of the dish surface area (20–40–80–100 $\mu g/cm^2$), for different time periods according to the test performed.

Cytotoxicity assay-lactate dehydrogenase leakage. The cytotoxic activity of the dusts was assessed investigating cell membrane integrity after 24 hours of particle exposure by measuring the leakage of lactate dehydrogenase (LDH) activity into the extracellular medium at a wavelength of 340 nm (37°C) with a microplate reader (Benchmark Plus; Bio-Rad). The procedure described in Polimeni *et al.* (2008) was followed. Both intracellular and extracellular enzyme activity was expressed as μmol of NADH oxidized/minute/dish, then extracellular LDH activity (LDH out) was calculated as a percentage of the total LDH activity (LDH tot = intracellular + extracellular) in the dish.

Morphological analysis by optical microscopy. BEAS-2B cells (0.1×10^6) were incubated for 96 hours with the dusts at the concentration of 20 $\mu g/cm^2$. Cells were then washed with PBS and observed with a Leica DC100 microscope (Leica Microsystems GmbH, Wetzlar, Germany) in order to perform a preliminary coarse evaluation of cell morphology parameters after particle incubation. For each experimental point, a minimum of 5 microscopic fields was examined.

Cytosolic and nuclear extracts. Cytosolic and nuclear extracts were obtained with the Nuclear Extraction Kit (Active Motif; Vinci-Biochem, Florence, Italy), according to the manufacturer's recommendations. The protein content of cellular lysates was assessed with the BCA kit.

Quantitative real-time PCR. Total RNA (2 μg) was reverse transcribed into cDNA using the iScript cDNA synthesis kit (Bio-Rad), and quantitative real-time PCR (qRT-PCR) was performed using IQTM SYBR Green Supermix (Bio-Rad). The same cDNA preparation was used for quantification of human E-cadherin, vimentin, α-smooth muscle actin (α-SMA), and the housekeeping gene ribosomal subunit protein S14. The relative quantification of each sample was performed comparing each PCR gene product with the S14 product using the Gene Expression Macro (http://www3.bio12rad.com/LifeScience/jobs/2004/04-/genex.xls; Bio-Rad). Primers used were as follows: S14 (forward: 5'-AGGTGCAAGGAGCTGGGTAT-3'; reverse: 5'-TCCAGGGGTCTTGGTCCTATTT-3'), E-cadherin (forward: 5′-TACGCCTGGGACTCCACCTA-3'; reverse: 5′-CCAGAAACGGAGGCCTGAT-3'), α-SMA (forward: 5′-GACAATGGCTCTGGGCTCTGTAA-3'; reverse: 5′-ATGCCATGTTCTATCGGGTACTTCA-3'), vimentin (forward: 5′-AGGAAATGGCTCGTCACCTTCGTGAATA-3'; reverse: 5′-GGAGTGTCGGTTGTTAAGAACTAGAGCT-3').

Western blotting. Aliquots of cytosolic extracts (10 μg) were separated by SDS-PAGE (8%–10%–12%). The blots were probed with anti-human antibodies and then with horseradish peroxidase–conjugated antibodies diluted in PBS-0.1% Tween with 5% Blocker Not-Fat Dry Milk. Proteins were detected by enhanced chemiluminescence using a ChemiDoc MP system (Bio-Rad) with Image Lab image acquisition. Glyceraldehyde 3-phosphate dehydrogenase (GAPDH) expression was used as loading control.

Antibodies. Primary antibodies to E-cadherin and GAPDH were purchased from Santa Cruz Biotechnology Inc (Santa Cruz, CA); primary antibody to vimentin was from Sigma; primary antibody to α-SMA was from GeneTex (Irving, CA). Secondary horseradish peroxidase–conjugated anti-rabbit or anti-mouse antibodies were from goat (Bio-Rad).

Statistical Analysis

Results are presented as mean ± SEM or SD, as indicated. Differences between groups were analyzed by 1-way ANOVA followed by Tukey's post hoc test (software: SPSS 21.0 for Windows; SPSS Inc, Chicago, IL). Differences with $P < .05$ were considered statistically significant.

RESULTS

Morphological and Chemical Characterization of Artificial Stone Dusts

The SEM images of artificial stone dusts 1 and 2, and of Qz (Min-U-Sil 5) are reported in Figure 1. The dusts generated by both types of processing (wet and dry) exhibited irregular shapes and sharp edges similarly to the reference quartz. Artificial stone dusts also showed conchoidal fractures and roughness typical of quartz obtained by grinding (Fubini, 1998a; Margolis and David, 1974). Opposite to the reference quartz, particles produced during artificial stone processing showed a minor amount of small particles stuck on the surface of the bigger ones, probably due to a difference in the electrostatic interaction.

Particle size of samples 1, 2, and 8 measured by automated flow particle image analysis (FPIA) is reported in Table 2. All samples contained 90% of particles with average diameter < 4 μm, calculated as the diameter of a circle of equivalent area to the particle (the circle equivalent or CE diameter). The average diameters were around 2 μm, the dry cutting resulting in a slightly finer dust than wet processing. In general, artificial stone dusts were coarser than the reference quartz Qz(Min-U-Sil 5). The SD associated with the average diameter of artificial stone dusts was higher than that of the reference quartz, meaning a higher heterogeneity in size. This heterogeneity was also confirmed by SEM images (Supplementary Figure S1) and size

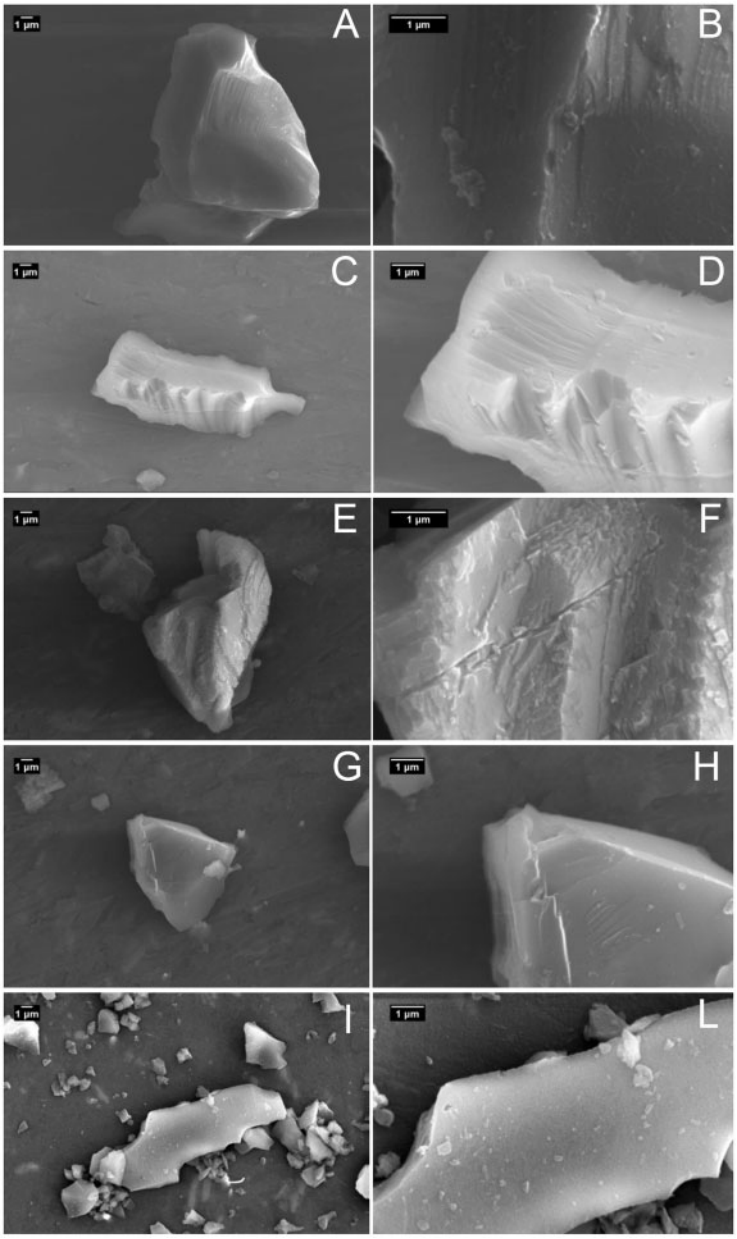

FIG. 1. SEM images of artificial stone dusts 1-wet (A and B), 1-dry (C and D), 2-wet (E and F), 2-dry (G and H), and the reference quartz Qz(Min-U-Sil 5) (I and L).

frequency distribution curves measured by FPIA (Supplementary Figure S2), which both revealed the presence of a coarse fraction around 10 μm. Accordingly, the specific surface area of sample 1 (wet and dry) was around 1.0 m^2/g and was lower than the specific surface area of the reference sample (5.1 m^2/g) (Table 2).

The elemental composition relative to Si content of artificial stone dusts is reported in Table 3 for samples 1 and 2 (wet and dry) and sample 8-dry, in Supplementary Table S1 for samples from 3- to 7-dry. All artificial stone dusts examined revealed high content of Si (approximately from 80% to 98%), except sample 2-wet (about 60%). Large differences in terms of minor elements were observed among the samples. Al was often present in different amounts, depending also from the type of cutting. Alkaline metals (K and Na) and alkaline earth metals (Ca and Mg) were found in all samples even in large percentages, especially K and Ca; remarkable is the amount of Ca in sample 2-wet and of K in sample 8-dry. Transition metals such as Fe, Cu, Zn, and Ti were also detected in traces or in larger content, depending on the sample.

Artificial Stone Dusts Showed a Robust Potential to Generate Oxygen and Carbon-Centered Free Radicals Strongly Dependent Upon the Working Process (Dry or Wet Cutting) and Aging

Artificial stone dusts were evaluated for their potential to generate free radicals in aqueous suspensions reproducing the cellular environment (Fubini and Hubbard, 2003; Fubini *et al*, 1995b). All samples were tested for their ability to generate hydroxyl radicals (HO˙) from hydrogen peroxide and carboxyl radicals (COO^-) from sodium formate used as a model molecule for the

TABLE 2. Particle Size and Specific Surface Area of Artificial Stone Dusts

Sample	Particle Size (μm)[a]		Specific Surface Area (m^2/g)[b]
	Average Diameter ± SD	90% Value	
1-wet	2.2 ± 3.8	3.6	0.8 ± 0.1
1-dry	1.9 ± 2.2	2.9	1.0 ± 0.1
2-wet	2.1 ± 3.3	3.8	ND
2-dry	1.7 ± 3.4	3.8	ND
8-dry	1.9 ± 1.4	3.0	ND
Qz(Min-U-Sil 5)	1.4 ± 0.6	2.0	5.1 ± 0.45

ND, not determined.
[a]Particle size was evaluated by FPIA which measures the average diameter expressed as circle equivalent (CE) diameter ± SD. The 90% value is the value of the CE diameter below which 90% observations fall.
[b]Specific surface area was evaluated by BET.

TABLE 3. Elemental Composition of Artificial Stone Dusts by μ-XRF

Sample	Element wt%/Si wt%						
	Al	K	Ca	Ti	Fe	Cu	Zn
1-wet	0.95	0.49	0.81	< 0.1%	0.38	0.12	–
1-dry	–	0.34	0.82	< 0.1%	0.60	0.36	–
2-wet	2.22	0.96	52.68	1.08	1.87	0.23	–
2-dry	–	0.80	0.51	0.38	0.34	0.24	–
8-dry	4.35	11.34	–	3.13	0.27	0.34	0.16
Qz(Min-U-Sil 5)	1.53	–	–	–	0.29	–	–

Notes: data are reported as weight percent of each detected element normalized by the amount of Si.

homolytic cleavage of C-H bonds in organic biomolecules. The yield of free radicals was monitored at different timing points (10, 30, and 60 minutes). The EPR signal associated with the $[DMPO\text{-}OH]^{\cdot}$ or $[DMPO\text{-}COO]^{\cdot-}$ adducts was double integrated to obtain the kinetic curves reported in Figure 2 and Supplementary Figure S3. Artificial stone dusts 1 and 2 showed a high potential to generate $HO^{\cdot}$ radicals (Figs. 2A and B), especially after 10 minutes of incubation when they were much more reactive than Qz(Min-U-Sil 5). However, opposite to Qz(Min-U-Sil 5), the rate of $HO^{\cdot}$ formation due to artificial stone dusts decreased over time, and after 60 minute the yield of $HO^{\cdot}$ radicals was close to that of Qz(Min-U-Sil 5) or even lower. There was no significant difference between the amount of $HO^{\cdot}$ radicals released by the samples obtained by wet (Figure 2A) or dry (Figure 2B) cutting. Instead, a large variation was observed in their ability to cleave the C-H bonds. Artificial stone dusts obtained by wet processing did not generate carboxyl radicals (Figure 2C), whereas dry processing produced highly reactive dusts, up to 10 times more than the reference Qz(Min-U-Sil 5) (Figure 2D). The kinetics of $COO^{\cdot-}$ radical formation for artificial stone dusts was complex, but in general it was more sustained over time than the kinetics of $HO^{\cdot}$ release even if a decrease after 60 minute of incubation was observed for both artificial stone dusts 1 and 2. The same trend was observed for the samples 3, 4, 5, 6, and 7, with few exceptions (Supplementary Figure S3). The high SD recorded for some samples is noteworthy, and probably due to the high heterogeneity in composition of these materials.

The yield in $COO^{\cdot-}$ radicals was also measured for 1 sample (8-dry) just after cutting the artificial stone and after 2, 8, and 15 days. Figure 2E shows a progressive reduction in the ability to generate $COO^{\cdot-}$ radicals by ageing of the dust, as known in literature for $HO^{\cdot}$ radicals from quartz (Vallyathan *et al.*, 1988). In particular, a remarkable decrease was observed up to 8 days from cutting then the amount of $COO^{\cdot-}$ radicals released became stable.

Artificial Stone Dusts Showed Absence of Hemolytic Activity and Slight Cytotoxic Effect Only on Human Bronchial Epithelial Cells

Artificial stone dusts were tested on purified human RBCs to evaluate their membranolytic activity (hemolysis), and on MH-S and BEAS-2B cells to assess the leakage of intracellular LDH into the extracellular medium, taken as an index of augmented cell membrane permeability and cytotoxicity. Artificial stone dusts were inactive in inducing RBC lysis at any of the concentrations investigated as shown in Figures 5A and B for samples 1-wet and 1-dry, respectively. No difference was observed between the 2 types of processing, and the same inactivity was also found for samples 2 and 4 (data not shown).

Although MH-S cells incubated for 24 hours with increasing concentrations of artificial stone dusts did not elicit any significant cytotoxicity (data not shown), BEAS-2B cells showed a low increase in LDH activity into the extracellular medium as reported in Figure 3 for sample 1 (both wet and dry). The increment was significant only with the dry sample. Surprisingly, the freshly generated dust (8-dry) did not show any hemolytic activity or cytotoxic effect (data not shown for brevity).

Among the cellular models used, BEAS-2B cells were more sensitive to contact with artificial stone dusts and were therefore selected as primary cells for subsequent experiments.

Removal of the Resin From Artificial Stone Dusts Revealed a Strong Hemolytic Activity and Cytotoxic Effect on Human Bronchial Epithelial Cells

In order to verify the presence on the particle surface of residues of a polymeric resin, one of the main components with quartz of artificial stone, which could affect the biological activity, sample 1 was analyzed under O_2 atmosphere by TGA coupled on-line with FTIR and Gas Chromatography Mass Spectrometry (GC-MS) analysis. The thermal behaviors of samples 1-dry and 1-wet are reported in Figure 4A and Supplementary Figure S4, respectively. The thermogram of sample 1-dry shows an overall weight loss of about 8% and is characterized by 3 processes, the first one, which occurred at lower temperature and was responsible for a negligible weight loss, was assigned to the desorption of water as confirmed by FTIR analysis; the second one identified by a well-defined minimum peak on the derivative curve, started at about 150°C and continued up to 450°C where a second process of lower extent took place. The correspondent derivative curve attained the zero value at about 570°C. The thermogram of sample 1-wet was similar to sample 1-dry, even if the weight loss was lower (5.5%) (Supplementary Figure S4). The resultant weight loss is in agreement with the nominal content of resin (5%–8%) and conceivably corresponds to the oxidative degradation of the polymeric resin.

The TGA analysis was repeated under dynamic N_2 atmosphere (Figure 4B) up to 900°C, and the evolved species were monitored with FTIR and GC-MS. Three weight loss processes were observed: a first one, characterized by a very broad minimum on the derivative curve, involved a slight weight loss, attributed to the desorption of H_2O; a main second process, with a

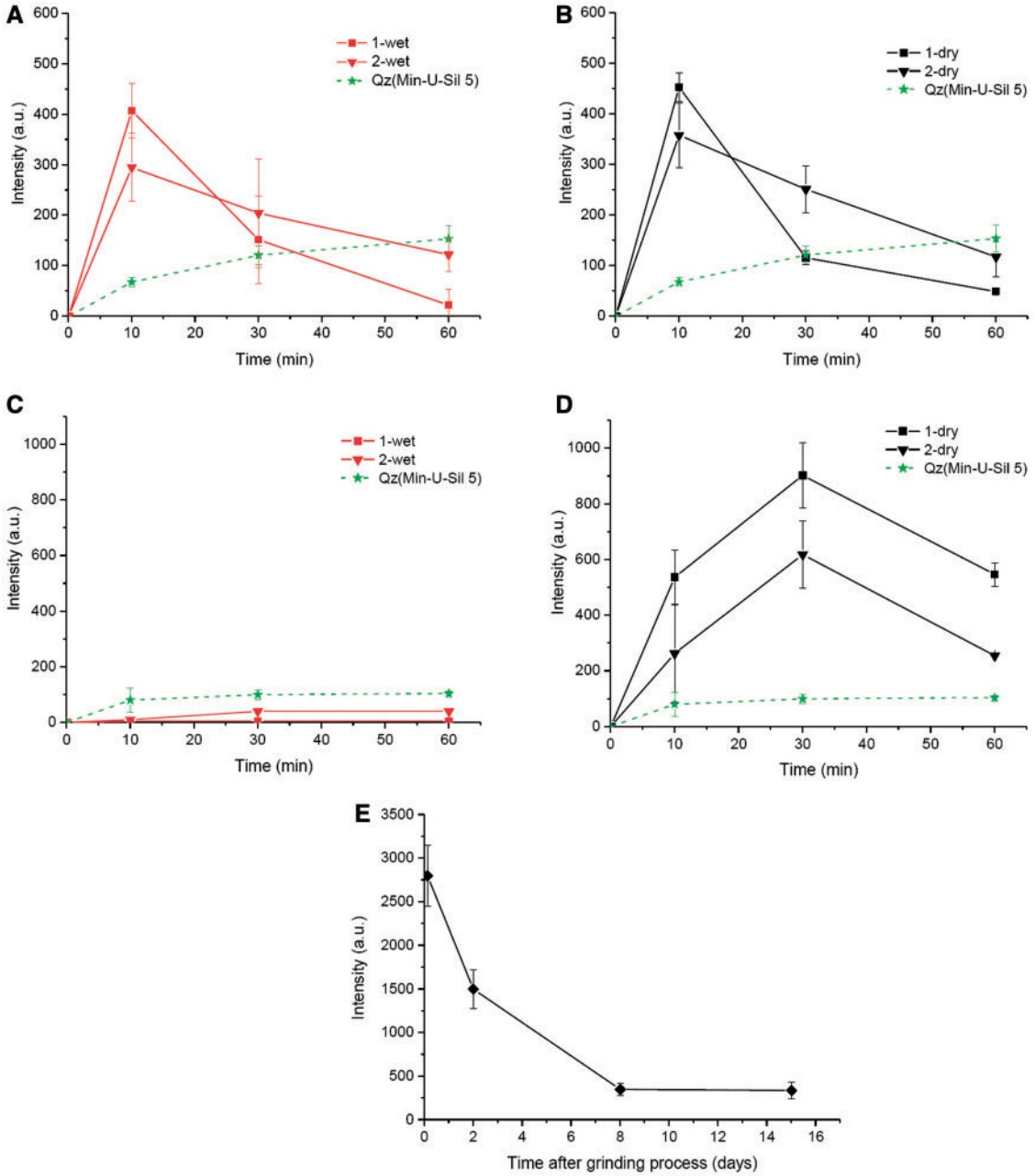

FIG. 2. Effect of the working process and of the ageing of the dusts on free radical generation. Kinetics of formation of hydroxyl (HO) (A and B) and carboxyl (COO^{-}) radicals (C and D) after incubation of artificial stone dusts 1 and 2 obtained by wet (A and C) or dry processing (B and D) with 5,5'-dimethyl-1-pirroline-N-oxide (DMPO) as trapping agent and hydrogen peroxide or sodium formate as target molecules, respectively. The amount of radicals released was measured after 10, 30, and 60 minute of incubation and is proportional to the intensity of the Electron Paramagnetic Resonance signal of the $[DMPO\text{-}OH]^{\cdot}$ or $[DMPO\text{-}COO]^{\cdot-}$ adducts measured by double integration and reported as arbitrary units. E, Amount of carboxyl (COO^{-}) radicals generated by sample 8-dry after 3 hours, and 2, 8, and 15 days after preparation (dry cutting in laboratory of an artificial stone). The results for artificial stone dusts are compared with the reference quartz Qz(Min-U-Sil 5) and are reported as mean ± SD of 3 independent experiments ($n = 3$).

well-resolved minimum peak on the derivative curve at ca. 450°C; a third process occurring at higher temperature and involving a negligible weight loss. The FTIR spectrum (Figure 4C) and the gas chromatogram (Figure 4D) of the gas evolved at 450°C confirmed the organic nature of the products released during degradation of sample 1-dry. The presence of toluene, styrene, and α-methylstyrene is indeed consistent with the degradation of an unsaturated polyester resin (Kandare *et al.*, 2008). Sample 1-wet showed the same FTIR-GC/MS profiles of sample 1-dry (data not reported for brevity).

Based on TGA curves, sample 1-wet and 1-dry were heated at 500°C in order to remove the resin, and a fraction of these samples was also ground in a ball mill in order to simulate the material abrasion during processing. Particle size was only partially affected by the thermal treatment. Conversely, a slight decrease of the average diameter and an increase of the BET area were observed after milling (Supplementary Table S2), as expected.

RBCs and BEAS-2B cells were incubated with increasing concentrations of artificial stone dusts untreated (1-wet and 1-dry)

or heated (h) or heated and then ground (h/g). After heating, both samples showed a significant increase of the hemolytic activity if compared with the starting material (Figs. 5A and B). On BEAS-2B cells, the increase was less evident (Figs. 5C and D) as only sample 1-wet(h) showed a significant increment of LDH leakage (Figure 5C). After heating and grinding, both the hemolytic activity (Figs. 5A and B) and the cytotoxicity (Figs. 5C and D) induced by artificial stone dusts increased with respect to untreated samples.

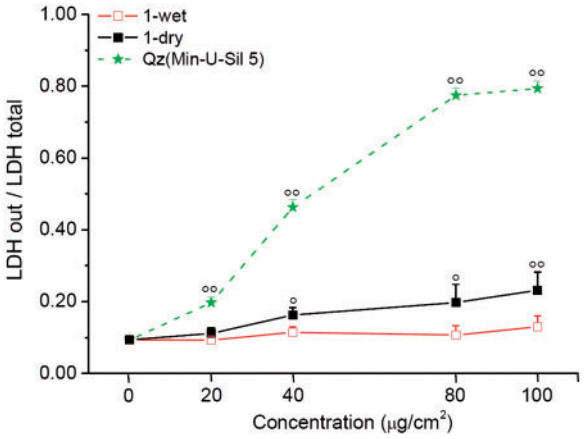

FIG. 3. Effect of artificial stone dusts (sample 1 dry and wet) on lactate dehydrogenase (LDH) release into the extracellular medium of bronchial epithelial (BEAS-2B) cells. Cells were incubated for 24 hours in either the absence (0 μg/cm^2, control) or presence of sample 1-wet, sample 1-dry or reference quartz Qz(Min-U-Sil 5) at the concentration of 0, 20, 40, 80, and 100 μg/cm^2. After a 24-hour incubation, LDH activity was calculated as percentage of total LDH activity of the dish. Data are presented as mean ± SEM of 3 independent experiments ($n = 3$). Significant differences versus control °$P < .001$, °°$P < .0001$.

Chronic Exposure to as-Abraded or resin-Deprived Artificial Stone Dusts Induce Epithelial-Mesenchymal Transition in Human Bronchial Epithelial Cells

Microscope images of BEAS-2B cells incubated for 96 hours with 20 μg/cm^2 of artificial stone dusts (sample 1, wet and dry, before and after the different treatments) are reported in Figure 6. After 96 hours, no LDH leakage was observed (data not reported for brevity). Cells exposed to untreated samples had completely lost their organization in compact islets, taking on a tapered and spindle shape with pointed ends and elongated protrusions, assuming a fibroblast-like appearance with cells arranged in parallel, whereas control cells reached confluence and showed their typical epithelial morphology. The same morphology alteration was observed in BEAS-2B cells incubated with samples 2 and 4 (Supplementary Figure S5).

To assess whether EMT could be the mechanism behind these changes, we examined the expression of classic epithelial and mesenchymal markers using qRT-PCR and Western blotting (WB) in BEAS-2B cells exposed to 20 μg/cm^2 of (wet and dry) sample 1. As shown in Figure 7A, qRT-PCR data indicated that (wet and dry) sample 1 significantly enhanced the messenger RNA (mRNA) expression of the mesenchymal markers vimentin and α-SMA. At the same time the mRNA expression of E-cadherin—a typical epithelial molecule of cellular adherent

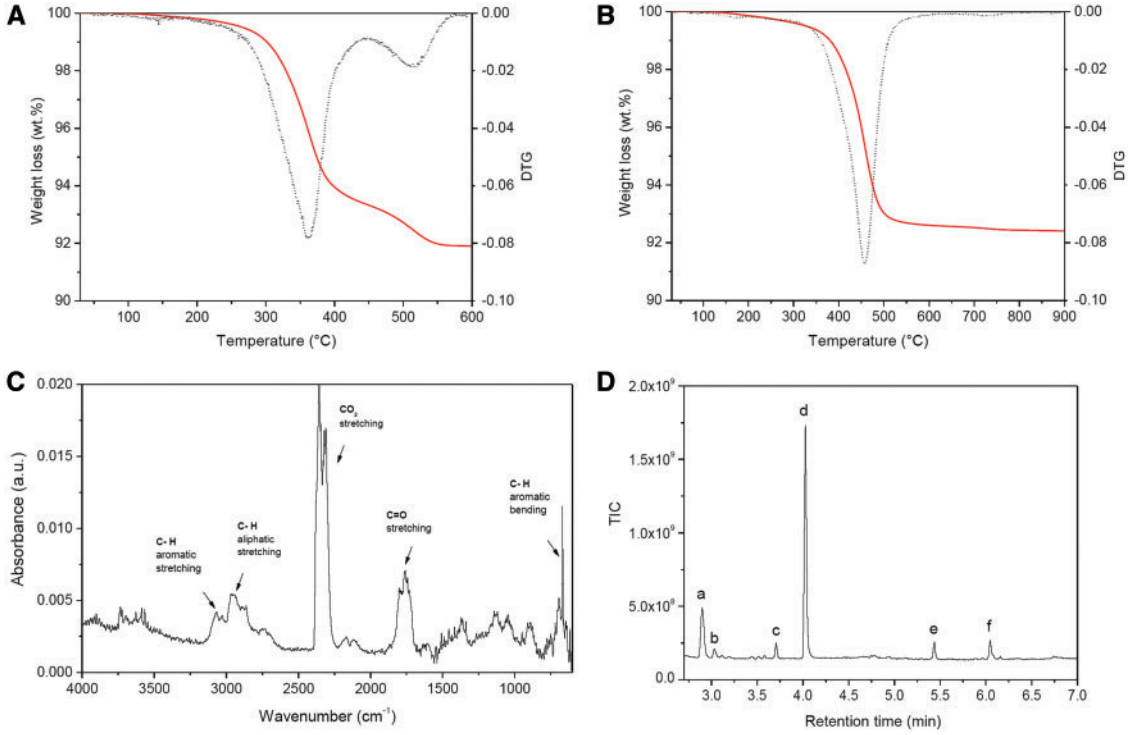

FIG. 4. Thermogravimetric (TGA)-Fourier Transform Infrared Spectroscopy (FTIR)-Gas Chromatography Mass Spectrometry (GC-MS) analysis of artificial stone dust 1-dry. A, Thermogravimetric (solid line) and derivative (dotted line) curves of sample 1-dry heated up to 600 °C under oxygen atmosphere. The TGA analysis evidenced an overall weight loss of about 8 wt.% in agreement with the content of resin declared by the manufacturer. B, TGA (solid line) and derivative (dotted line) curves of sample 1-dry heated up to 900 °C under nitrogen atmosphere. C, FTIR spectra in the 4000–600 cm^{-1} spectral region and (D) gas chromatogram of the volatiles generated from thermal degradation of sample 1-dry at 450 °C under nitrogen atmosphere. The FTIR and GC-MS profiles were consistent with a polystyrene resin. GC chromatographic peaks correspond to: (a) toluene at 2.89 minutes, (b) 3-methylheptane at 3.03, (c) ethylbenzene at 3.70 minutes, (d) styrene at 4.03 minutes, (e) α-methylstyrene at 5.44 minutes, and (f) 2-ethyl-1-hexanol at 6.03 minutes.

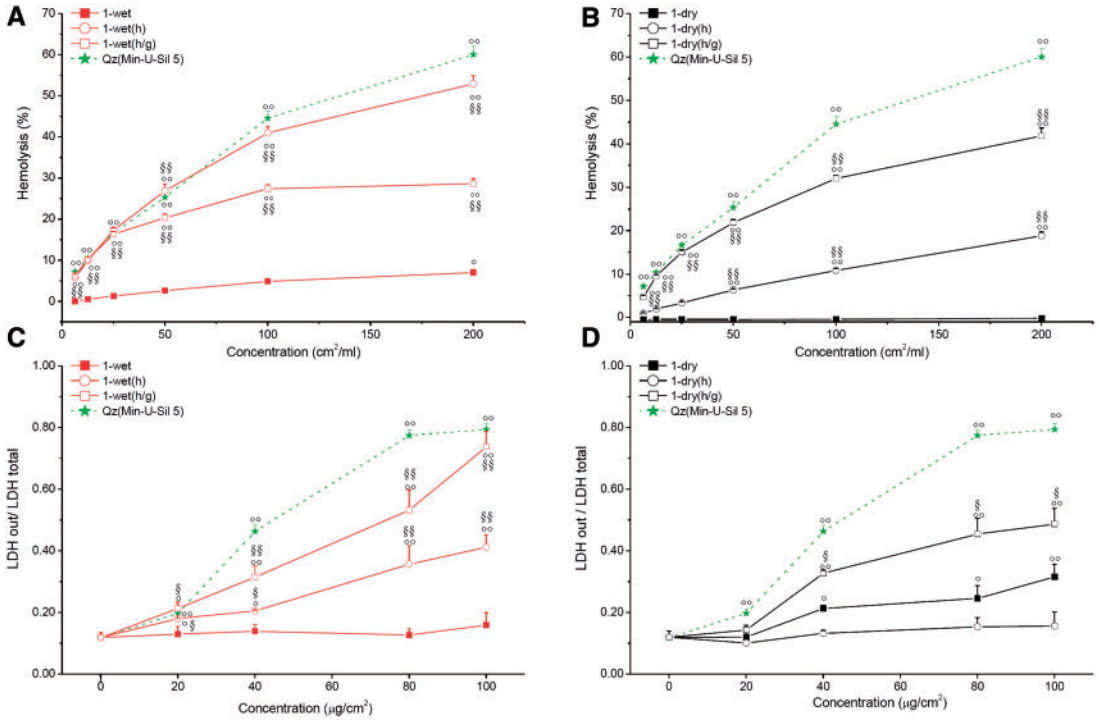

FIG. 5. Effect of resin removal on the hemolytic activity (A and B) and bronchial epithelial (BEAS-2B) cytotoxicity (C and D) of artificial stone dusts (samples 1-wet and 1-dry). A and B, red blood cells (RBCs) were incubated with increasing concentrations of sample 1 untreated, sample 1(h), sample 1(h/g) or reference Qz(Min-U-Sil 5) quartz and hemolytic activity was assessed. C and D, lactate dehydrogenase (LDH) release into the extracellular medium of BEAS-2B cells. Cells were incubated for 24 hours in either the absence (0 μg/cm^2, control) or presence of sample 1 untreated, sample 1(h), sample 1(h/g) or reference Qz(Min-U-Sil 5) quartz at the concentration of 0, 20, 40, 80, and 100 μg/cm^2. After a 24-hour incubation, LDH activity was calculated as percentage of total LDH activity of the dish. Data are presented as mean ± SEM ($n = 3$). Significant differences versus control $^{\circ}P < .001$, $^{\circ\circ}P < .0001$; versus untreated sample $^{\S}P < .001$, $^{\S\S}P < .0001$.

junctions—was significantly repressed. WB showed a significantly increased expression of vimentin and α-SMA, more marked with sample 1-wet, and loss of E-cadherin after incubation with (wet and dry) sample 1 (Figure 7B). Artificial stone samples were compared with the positive control Qz (Min-U-Sil 5) and MSS as negative control.

BEAS-2B cells exposed to heated (h) or heated and then ground (h/g) samples assumed a fibroblast-like appearance as BEAS-2B cells exposed to untreated samples (Figure 6). Similarly, qRT-PCR data indicated that both treatments altered the mRNA expression of vimentin and E-cadherin with respect to control cells to almost the same extent of the cells exposed to untreated samples (Figure 7A). In agreement, also WB data showed that the expression of vimentin and E-cadherin proteins in BEAS-2B cells was very similar to that found for the untreated samples (Figure 7B). Finally, α-SMA mRNA and protein levels increased for BEAS-2B cells exposed to treated samples with respect to control, even if only a modest increment was observed for the treated samples 1-wet(h) and 1-wet(h/g).

DISCUSSION

The unusual severity of the silicosis observed even in young workers within relatively short time of exposure (Pérez-Alonso *et al.*, 2014) led to suppose that peculiar physicochemical properties and atypical surface features may drive the detrimental effects of artificial stone dusts (Paolucci *et al.*, 2015). Indeed, although composed mainly by crystalline silica, artificial stones contain other components, both organic and inorganic, which may modify the well-known reactivity of quartz (Fubini, 1998b). To date, no study has been performed on the physicochemical characteristics of artificial stone dusts or on the cellular effects elicited by this type of particles.

In the present research, a set of dusts obtained from both dry and wet cutting of artificial stones has been considered. The dusts here examined showed size and morphology typical of mineral quartz dusts obtained by grinding. Besides the high content (ca. 80%–98%) of quartz, our data indicated that residues of the polymeric resin used as conglomerant in the manufacture of the artificial stones were retained on the surface of the particles. K, Na, Ca, Mg, Fe, Cu, Zn, and Ti in different amounts were also found and may be associated to included pigments or to the cutting material.

Artificial stone dusts exhibited a strong potential to generate free radicals, mainly hydroxyl radicals, in acellular systems mimicking the cellular environment. Free radicals are highly reactive species involved in genotoxicity, and in inflammatory and fibrotic responses induced by quartz particles (Castranova, 2004; Fubini and Hubbard, 2003; Knaapen *et al.*, 2004; Øvrevik *et al.*, 2015). The reactivity in HO˙ generation did not depend on the origin of the dust (no significant difference between dry and wet samples was observed) and largely exceeded that of the most part of quartz currently used in experimental studies (Pavan *et al.*, 2013; Schins *et al.*, 2002), Min-U-Sil 5 included. A similar high reactivity was observed by Clouter *et al.* (2001) for 2 workplace quartz and was explained by the large presence of redox active transition metals, such as Fe and Cu, able to trigger the Fenton reaction (Fubini and Hubbard, 2003). Opposite to HO˙ generation, COO^{-} release varied from dry to wet samples. Wet-processing completely abolished the reactivity toward C-H bond likely by reducing the formation of surface radicals, which are present in large amount on silica surfaces fractured in a dry

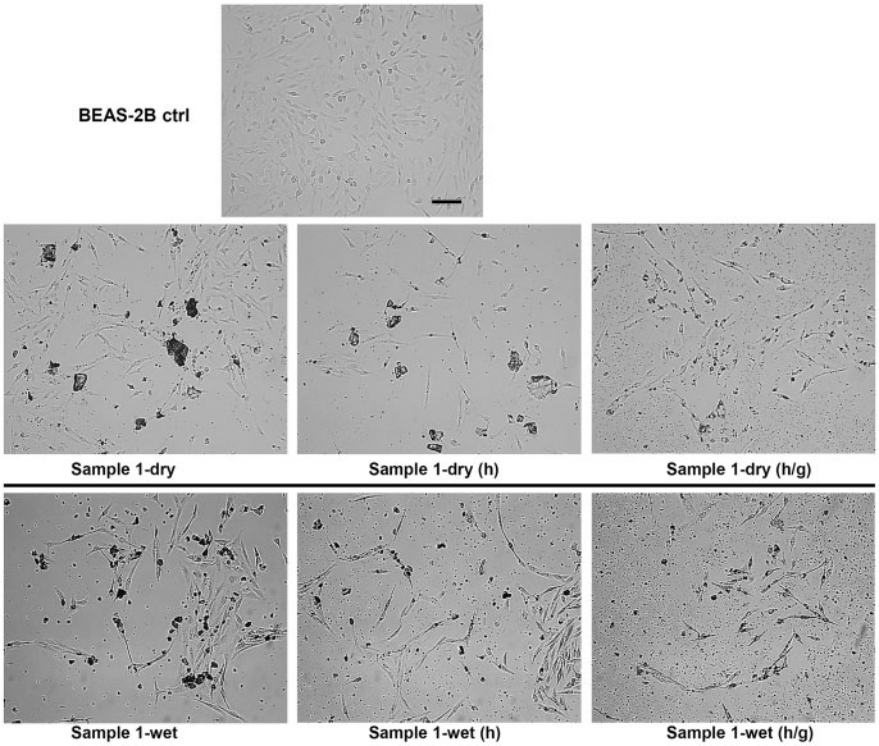

FIG. 6. Representative microscope images of bronchial epithelial (BEAS-2B) cells exposed to artificial stone dusts. Cells were incubated for 96 hours in either the absence (0 $\mu g/cm^2$, ctrl) or the presence of 20 $\mu g/cm^2$ of sample 1 untreated (1-wet and 1-dry), heated (h) or heated and then ground (h/g). After the incubation, cells were rinsed with PBS and observed by optical microscopy. Representative images are shown ($\times$10; scale bar = 50 μm).

oxygen atmosphere (Fubini *et al.*, 1989,1995a), and/or by oxidizing surface metals. As instance, Fe(III) was unreactive in catalyzing $COO^{\cdot-}$ generation opposite to Fe(II) (Tomatis et al., 2002).

Surface radicals rapidly decay, even if traces of these are usually visible on aged dusts (Fubini *et al.*, 1990), thus their amount is expected to be higher in recently cleaved than in aged quartz surfaces (Vallyathan *et al.*, 1988). This explains the high reactivity of the sample 8-dry in $COO^{\cdot-}$ release when tested few hours after cutting and then the progressive decrease of the amount of radicals over time. This also suggests that the ability of the samples here analyzed to catalyze free radical generation is lower than that of the fresh particles inhaled by workers.

Despite the high radical reactivity, classic *in vitro* endpoints commonly observed for a number of crystalline silica particles (International Agency for Research on Cancer (IARC), 1997) did not showed marked signs of cellular toxicity. Neither hemolytic activity nor cytotoxic effect on murine MH-S were observed. Only a slight cytotoxicity was observed on human bronchial epithelial cells. Moreover, the hemolytic activity and cytotoxicity of the freshly generated dust (sample 8-dry) did not significantly differ from those of the other samples. This is somewhat surprising given that in general freshly fractured surfaces are more cytotoxic than aged ones (Vallyathan *et al.*, 1991). The cellular inertness here observed may be ascribed to the presence of a polymeric resin that partially covers particle surface, preventing the interaction with cells without affecting the reactive surface sites involved in free radical generation. Similarly, it has been reported a reduction of the hemolytic and macrophage stimulatory activity of quartz after coating with an organosilane (Vallyathan *et al.*, 1991). After degradation of the resin by a thermal treatment, a substantial hemolytic activity appeared for sample 1 (both dry and wet), as well as a cytotoxic effect for sample 1-wet. As expected, cytotoxicity further increased for dusts heated and then ground. The occurrence of a significant hemolytic activity after degradation of the polymeric resin confirms that particle surface needs to be accessible in order to interact with membranes, and that hemolysis is unrelated to free radical generation (Pavan *et al.*, 2013). The present data suggest that some of the classic endpoints used for evaluating *in vitro* quartz toxicity, such as cytotoxicity and hemolytic activity, may not be adequate to describe the biological activity of complex quartz-containing dusts. We may not exclude that in the long-term, a chronic permanence of artificial stone dusts in lung lining fluid may induce a degradation of the resin and expose the naked particle surface thus restoring the cytotoxic and membranolytic activity of quartz dust.

Contrary to hemolysis and cytotoxicity, EMT took place for all samples tested, regardless the presence of the resin. Epithelial-mesenchymal transition has been recently recognized as an important pathway in fibrosis. Differentiated epithelial cells may play an important role in the regulation of lung fibrosis by producing cytokines and growth factors (Guarino *et al.*, 2009) or may undergo transition to a mesenchymal phenotype, giving rise to generation of fibroblasts and myofibroblasts (Tanjore *et al.*, 2009). An altered expression of adhesion molecules and the EMT was first observed *in vivo* by Blanco demonstrating an association with silica-induced lung carcinogenesis in rats (Blanco *et al.*, 2004). Recently, the EMT process was observed *in vitro* in human bronchial epithelial cells (Gao et al., 2011), and in human lung epithelial (A549) and BEAS-2B cells exposed to crystalline silica (Rong *et al.*, 2015). Finally, Antognelli demonstrated that Min-U-Sil 5 was able to induce EMT in BEAS-2B cells and that acquisition of an EMT-like phenotype was associated with a neoplastic-like cell transformation process

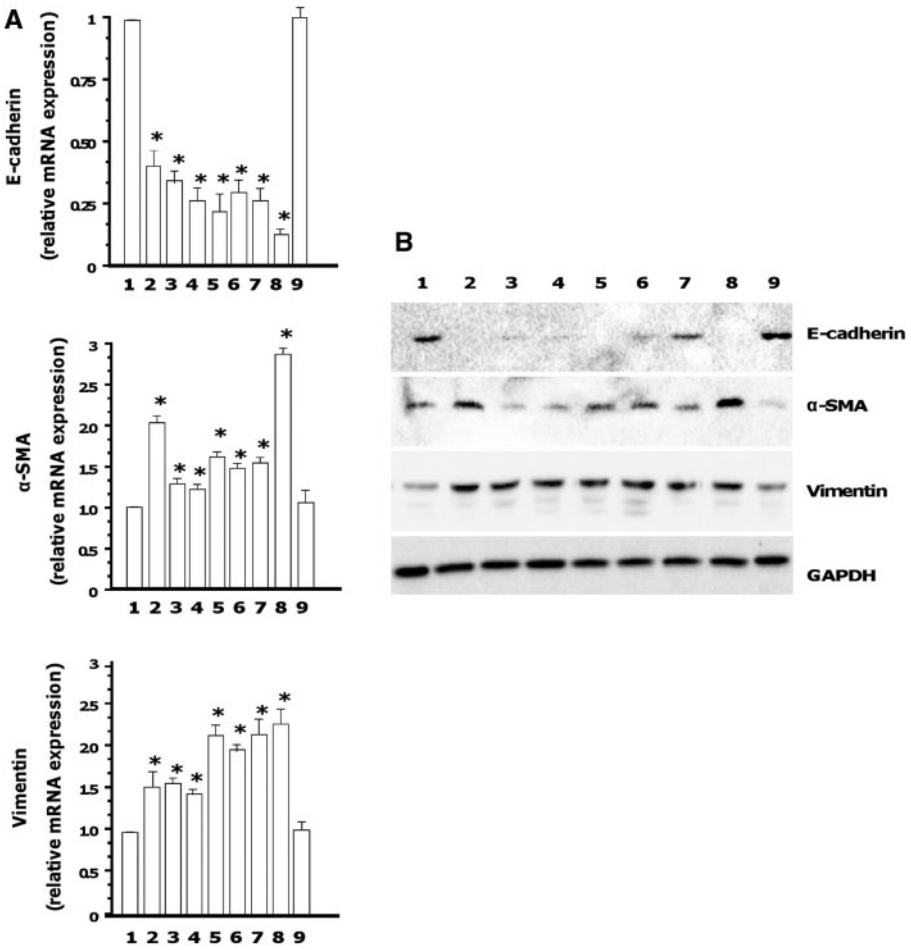

FIG. 7. Relative expression of epithelial and mesenchymal markers of bronchial epithelial (BEAS-2B) cells exposed to artificial stone dusts. Relative expression of epithelial and mesenchymal markers was checked by quantitative real-time PCR **(A)** and Western blotting **(B)**. BEAS-2B cells were incubated for 96 hours in either the absence (0 μg/cm^2, control) or presence of 20 μg/cm^2 of artificial stone dusts (lane 1 = control; lane 2 = sample 1-wet; lane 3 = sample 1-wet(h); lane 4 = sample 1-wet(h/g); lane 5 = sample 1-dry; lane 6 = sample 1-dry(h); lane 7 = sample 1-dry(h/g); lane 8 = Qz(Min-U-Sil 5); lane 9 = MSS). A, Expression of E-cadherin, α-SMA and vimentin mRNA. Results were expressed in units of relative mRNA expression compared with control cells ($n = 3$). versus control *$P < .0001$. B, Expression of E-cadherin, α-SMA and vimentin proteins. Glyceraldehyde 3-phosphate dehydrogenase (GAPDH) was used as loading control. Each figure is representative of 3 experiments giving similar results.

(Antognelli *et al.*, 2016), in agreement with recently findings from an *in vivo* study addressing the linkage of EMT-dependent tissue repair with neoplasia following silica exposure (Wang *et al.*, 2015).

EMT is a process by which epithelial cell-cell adhesions are dissolved, the actin cytoskeleton is reorganized, and cells acquire increased cell-matrix contacts and enhanced migratory and invasive capabilities (Yilmaz and Christofori, 2009). After 96 hours of incubation, noncytotoxic concentrations of artificial stone dusts were able to induce a significant morphological alteration of BEAS-2B cells. Exposed cells appeared spindle-shaped and disorganized. The shape change was accompanied, in both cases, by a significant loss of E-cadherin expression, a typical marker of epithelial cells, which is downregulated when cells lose their polarity and cell-cell contact (Thiery *et al.*, 2009). Moreover, transformed cells acquired mesenchymal characteristics such as a significant increase of cytoskeletal proteins (ie, vimentin) and rearrangement of actin with *de novo* synthesis of α-SMA, essential for enhanced motility and invasiveness (Thiery *et al.*, 2009). These events are not clearly related to a specific physicochemical feature of the sample. The induction of EMT may be related to the high reactivity in particle-derived generation of reactive oxygen species. The different treatments, ie, heating to expose free quartz surface, and heating followed by grinding, carried out on sample 1 (both dry and wet), did not modify the EMT response with respect to the pristine sample.

In conclusion, artificial stone dust may be a strong activator of fibrotic markers, as here suggested by the EMT, rather than a membranolysis inducer. The acquisition of the EMT-like phenotype was evident for all samples demonstrating the high fibrogenic activity of these dusts, regardless of the presence of the resin. The large amount of redox-active transition metal ions and the high content of quartz in artificial stone are responsible for the observed strong cell-free oxidative activity. Our study provides evidence that artificial stone workers are at risk of exposure to highly reactive and potentially fibrogenic dusts in respirable size. Cell-free oxidative tests confirmed that these dusts are much more reactive when freshly abraded at the time of cutting. These features may contribute, together with the high level of exposure recorded in workplaces, to the high incidence of silicosis reported by occupational survey and confirm the relevance of regulatory and preventive measures during processing of artificial stones.

SUPPLEMENTARY DATA

Supplementary data are available online at http://toxsci.oxfordjournals.org/.

ACKNOWLEDGMENTS

We gratefully acknowledge the Network Italiano Silice (NIS) who coordinates research and prevention in the field of silica pathogenicity and in particular Dr Fabio Capacci, Dept. di Prevenzione ASL Firenze, not only for the support to the research but also for suggesting the subject of artificial stone dust toxicity and providing useful information and discussions all along the development of the study. We kindly acknowledge Dr Carla Poli, Dept. di Prevenzione, USL 11 of Empoli (FI, Italy), and Dr Mariangela Azzone, Dept. di Prevenzione, ASL 19 of Asti (AT, Italy) for sample collection.

FUNDING

This work was supported by Italian Workers' Compensation Authority (Istituto Nazionale Assicurazione Infortuni sul Lavoro - INAIL) of Piemonte as a doctoral fellowship given to CP and by the Local Health Authority (Azienda Sanitaria Locale - ASL) of Firenze (Italy). Particle image analysis has been obtained with the equipment acquired by the Interdepartmental Center "G. Scansetti" for Studies on Asbestos and Other Toxic Particulates with a grant from Compagnia di San Paolo, Torino, Italy.

REFERENCES

Antognelli, C., Gambelunghe, A., Muzi, G., and Talesa, V. N. (2016). Glyoxalase I drives epithelial-to-mesenchymal transition via argpyrimidine-modified Hsp70, miR-21 and SMAD signalling in human bronchial cells BEAS-2B chronically exposed to crystalline silica Min-U-Sil 5: Transformation into a neoplastic-like phenotype. *Free Radic. Biol. Med.* **92**, 110–125. 10.1016/j.freeradbiomed.2016.01.009.

Bang, K. M., Mazurek, J. M., Wood, J. M., White, G. E., Hendricks, S. A., and Weston, A. (2015). Silicosis mortality trends and new exposures to respirable crystalline silica - United States, 2001-2010. *MMWR Morb. Mortal Wkly Rep.* **64**, 117–120.

Bartoli, D., Banchi, B., Di Benedetto, F., Farina, F. A., Iaia, T. E., Poli, C., Romanelli, M., Scancarello, G., and Tarchi, M. (2012). Silicosis in employees in the processing of kitchen, bar and shop countertops made from quartz resin composite. Provisional results of the environmental and health survey conducted within the territory of USL 11 of Empoli in Tuscany among employees in the processing of quartz resin composite materials and review of the literature. *Ital. J. Occup. Environ. Hyg* **3**, 138–143.

Blanco, D., Vicent, S., Elizegi, E., Pino, I., Fraga, M. F., Esteller, M., Saffiotti, U., Lecanda, F., and Montuenga, L. M. (2004). Altered expression of adhesion molecules and epithelial-mesenchymal transition in silica-induced rat lung carcinogenesis. *Lab. Invest.* **84**, 999–1012. 10.1038/labinvest.3700129.

Castranova, V. (2004). Signaling pathways controlling the production of inflammatory mediators in response to crystalline silica exposure: role of reactive oxygen/nitrogen species. *Free Radic. Biol. Med.* **37**, 916–925. 10.1016/j.freeradbiomed.2004.05.032.

Cho, W. S., Duffin, R., Bradley, M., Megson, I. L., MacNee, W., Lee, J. K., Jeong, J., and Donaldson, K. (2013). Predictive value of in vitro assays depends on the mechanism of toxicity of metal oxide nanoparticles. *Part. Fibre Toxicol* **10**, 15. 10.1186/1743-8977-10-55.

Clouter, A., Brown, D., Hohr, D., Borm, P., and Donaldson, K. (2001). Inflammatory effects of respirable quartz collected in workplaces versus standard DQ12 quartz: particle surface correlates. *Toxicol. Sci.* **63**, 90–98. 10.1093/toxsci/63.1.90.

Fenoglio, I., Martra, G., Prandi, L., Tomatis, M., Coluccia, S., and Fubini, B. (2000). The role of mechanochemistry in the pulmonary toxicity caused by particulate minerals. *J. Mater. Synth. Process* **8,** 4), 145–153, 10.1023/A. 1011303924468.

Friedman, G. K., Harrison, R., Bojes, H., Worthington, K., and Filios, M. (2015). Notes from the field: silicosis in a countertop fabricator - Texas, 2014. *MMWR Morb. Mortal Wkly Rep.* **64**, 129–130.

Fubini, B., Giamello, E., Pugliese, L., and Volante, M. (1989). Mechanically induced defects in quartz and their impact on pathogenicity. *Solid State Ionics* **32-3**, 334–343. 10.1016/0167-2738(89)90238-5.

Fubini, B. (1998a). Health effects of silica. In *The Surface Properties of Silica* (A. P. Legrand, Eds.), pp. 415–464. John Wiley and Sons, Chichester, UK.

Fubini, B. (1998b). Surface chemistry and quartz hazard. *Ann. Occup. Hyg* **42**, 521–530, 10.1016/s0003-4878(98)00066-0.

Fubini, B., Bolis, V., Cavenago, A., and Volante, M. (1995a). Physicochemical properties of crystalline silica dusts and their possible implication in various biological responses. *Scand. J. Work Environ. Health* **21**, 9–14.

Fubini, B., Giamello, E., Volante, M., and Bolis, V. (1990). Chemical functionalities at the silica surface determining its reactivity when inhaled - formation and reactivity of surface radicals. *Toxicol. Ind. Health* **6**, 571–598.

Fubini, B., Mollo, L., and Giamello, E. (1995b). Free-radical generation at the solid/liquid interface in iron-containing minerals. *Free Radical Res.* **23**, 593–614. 10.3109/10715769509065280.

Fubini, B., and Hubbard, A. (2003). Reactive oxygen species (ROS) and reactive nitrogen species (RNS) generation by silica in inflammation and fibrosis. *Free Radic. Biol. Med* **34**, 1507–1516. 10.1016/S0891-5849(03)00149-7.

Gao, Z., Hu, Y., Peng, J., Deng, Z., Liang, G., Jiang, H., and Zhou, J. (2011). ERK signaling pathway mediated epithelial-mesenchymal transition induced by SiO_2 in human bronchial epithelial cells. *Zhong Nan Da Xue Xue Bao Yi Xue Ban* **36**, 1085–1089. 10.3969/j.issn.1672-7347.2011.11.009.

García Vadillo, C., Gómez, J., and Morillo, J. (2011). Silicosis in quartz conglomerate workers. *Arch. Bronconeumol.* **47**, 53.

Gazzano, E., Ghiazza, M., Polimeni, M., Bolis, V., Fenoglio, I., Attanasio, A., Mazzucco, G., Fubini, B., and Ghigo, D. (2012). Physicochemical determinants in the cellular responses to nanostructured amorphous silicas. *Toxicol. Sci.* **128**, 158–170. 10.1093/toxsci/kfs128.

Ghiazza, M., Polimeni, M., Fenoglio, I., Gazzano, E., Ghigo, D., and Fubini, B. (2010). Does vitreous silica contradict the toxicity of the crystalline silica paradigm? *Chem. Res. Toxicol.* **23**, 620–629. 10.1021/tx900369x.

Ghiazza, M., Tomatis, M., Doublier, S., Grendene, F., Gazzano, E., Ghigo, D., and Fubini, B. (2013). Carbon in intimate contact with quartz reduces the biological activity of crystalline silica dusts. *Chem. Res. Toxicol.* **26**, 46–54. 10.1021/tx300299v.

Guarino, M., Tosoni, A., and Nebuloni, M. (2009). Direct contribution of epithelium to organ fibrosis: epithelial-mesenchymal transition. *Hum. Pathol.* **40**, 1365–1376. 10.1016/j.humpath.2009.02.020.

Hornung, V., Bauernfeind, F., Halle, A., Samstad, E. O., Kono, H., Rock, K. L., Fitzgerald, K. A., and Latz, E. (2008). Silica crystals

and aluminum salts activate the NALP3 inflammasome through phagosomal destabilization. *Nat. Immunol.* **9**, 847–856. 10.1038/ni.1631.

Hu Yong, B., Li Fei, F., Deng Zheng, H., and Pan Pin, H. (2015). Transcriptional factor snail mediates epithelial-mesenchymal transition in human bronchial epithelial cells induced by silica. *Biomed. Environ. Sci.* **28**(7), 544-548, 10.3967/bes2015.078.

Hughes, C. S., Colhoun, L. M., Bains, B. K., Kilgour, J. D., Burden, R. E., Burrows, J. F., Lavelle, E. C., Gilmore, B. F., and Scott, C. J. (2016). Extracellular cathepsin S and intracellular caspase 1 activation are surrogate biomarkers of particulate-induced lysosomal disruption in macrophages. *Part. Fibre Toxicol.* **13**, 19–10. 1186/s12989-016-0129-5.

International Agency for Research on Cancer (IARC) (1997). Silica, some silicates, coal dust and para-aramid fibrils. *In IARC Monographs on the Evaluation of Carcinogenic Risks to Humans*. **Vol 68**. IARC, Lyon, France.

International Agency for Research on Cancer (IARC) (2012). A review of human carcinogens: arsenic, metals, fibres, and dusts. In *IARC Monographs on the Evaluation of Carcinogenic Risks to Human*. Vol **100C**. IARC, Lyon, France.

Kandare, E., Kandola, B. K., Price, D., Nazare, S., and Horrocks, R. A. (2008). Study of the thermal decomposition of flame-retarded unsaturated polyester resins by thermogravimetric analysis and Py-GC/MS. *Polym. Degrad. Stabil.* **93**, 1996–2006, 10.1016. /j.polymdegradstab.2008.03.032.

Knaapen, A. M., Borm, P. J., Albrecht, C., and Schins, R. P. (2004). Inhaled particles and lung cancer. Part A: Mechanisms. *Int. J. Cancer* **109**, 799–809. 10.1002/ijc.11708.

Kramer, M. R., Blanc, P. D., Fireman, E., Amital, A., Guber, A., Rhahman, N. A., and Shitrit, D. (2012). Artificial stone silicosis: Disease resurgence among artificial stone workers. *Chest* **142**, 419–424, 10.1378. /chest.11-1321.

Li, L., and Li, W. (2015). Epithelial-mesenchymal transition in human cancer: comprehensive reprogramming of metabolism, epigenetics, and differentiation. *Pharmacol. Ther.* **150**, 33–46. 10.1016/j.pharmthera.2015.01.004.

Liang, D., Wang, Y., Zhu, Z., Yang, G., An, G., Li, X., Niu, P., Chen, L., and Tian, L. (2015). Increased expression of bone morphogenetic protein-7 and its related pathway provides an anti-fibrotic effect on silica induced fibrosis in vitro. *Toxicol. Res.* **4**, 1511–1522. 10.1039/c5tx00159e.

Lu, S. L., Duffin, R., Poland, C., Daly, P., Murphy, F., Drost, E., MacNee, W., Stone, V., and Donaldson, K. (2009). Efficacy of simple short-term in vitro assays for predicting the potential of metal oxide nanoparticles to cause pulmonary inflammation. *Environ. Health Perspect.* **117**, 241–247. 10.1289/ehp.11811.

Margolis, S. V. K., and David, H. (1974). Processes of formation and environmental occurrence of microfeatures on detrital quartz grains. *Am. J. Sci.* **274**, 449–464.

Martínez, C., Prieto, A., García, L., Quero, A., González, S., and Casan, P. (2010). Silicosis: a disease with an active present. *Arch. Bronconeumol.* **46**, 97–100, 10. 1016/j.arbres.2009.07.008.

Nowrin, K., Sohal, S. S., Peterson, G., Patel, R., and Walters, E. H. (2014). Epithelial-mesenchymal transition as a fundamental underlying pathogenic process in COPD airways: fibrosis, remodeling and cancer. *Expert Rev. Respir. Med* **8**, 547–559. 10.1586/17476348.2014.948853.

OSHA, NIOSH (2015). Hazard alert: Worker exposure to silica during countertop manufacturing, finishing and installation. Available at: http://www.cdc.gov/niosh/docs/2015-106/pdfs/2015-106.pdf. Accessed Feb 5, 2016.

Øvrevik, J., Refsnes, M., Låg, M., Holme, J. A., and Schwarze, P. E. (2015). Activation of proinflammatory responses in cells of the airway mucosa by particulate matter: oxidant- and non-oxidant-mediated triggering mechanisms. *Biomolecules* **5**, 1399–1440. 10.3390/biom5031399.

Paolucci, V., Romeo, R., Sisinni, A. G., Bartoli, D., Mazzei, M. A., and Sartorelli, P. (2015). Silicosis in workers exposed to artificial quartz conglomerates: does it differ from chronic simple silicosis? *Arch. Bronconeumol.* **51**, e57–e60.

Pascual, S., Urrutia, I., Ballaz, A., Arrizubieta, I., Altube, L., and Salinas, C. (2011). Prevalence of silicosis in a marble factory after exposure to quartz conglomerates. *Arch. Bronconeumol.* **47**, 50–51. 10.1016/j.arbres.2010.09.004.

Pavan, C., Rabolli, V., Tomatis, M., Fubini, B., and Lison, D. (2014). Why does the hemolytic activity of silica predict its pro-inflammatory activity? *Part. Fibre Toxicol.* **11**, 76. 10.1186/s12989-014-0076-y.

Pavan, C., Tomatis, M., Ghiazza, M., Rabolli, V., Bolis, V., Lison, D., and Fubini, B. (2013). In search of the chemical basis of the hemolytic potential of silicas. *Chem. Res. Toxicol.* **26**, 1188–1198. 10.1021/tx400105f.

Polimeni, M., Gazzano, E., Ghiazza, M., Fenoglio, I., Bosia, A., Fubini, B., and Ghigo, D. (2008). Quartz inhibits glucose 6-phosphate dehydrogenase in murine alveolar macrophages. *Chem. Res. Toxicol.* **21**, 888–894. 10.1021/tx7003213.

Pérez-Alonso, A., Córdoba-Doña, J. A., and Garcia-Vadíllo, C. (2015). Silicosis: relevant differences between marble workers and miners. *Arch. Bronconeumol.* **51**, 53–54.

Pérez-Alonso, A., Córdoba-Doña, J. A., Millares-Lorenzo, J. L., Figueroa-Murillo, E., García-Vadillo, C., and Romero-Morillos, J. (2014). Outbreak of silicosis in Spanish quartz conglomerate workers. *Int. J. Occup. Environ. Health* **20**, 26–32. 10.1179/2049396713Y.0000000049.

Rong, Y., Shen, Y., Zhang, Z., Cui, X., Xiao, L., Liu, Y., Luo, X., and Chen, W. (2015). Blocking TGF-β expression inhibits silica particle-induced epithelial-mesenchymal transition in human lung epithelial cells. *Environ. Toxicol. Pharmacol.* **40**, 861–869. 10.1016/j.etap.2015.09.014.

Sauvé, J. F. (2015). Historical and emerging workplaces affected by silica exposure since the 1930 Johannesburg conference on Silicosis, with special reference to construction. *Am. J. Ind. Med* **58(Suppl. 1)**, 67–71. 10.1002/ajim.22507.

Schins, R. P., Knaapen, A. M., Cakmak, G. D., Shi, T., Weishaupt, C., and Borm, P. J. (2002). Oxidant-induced DNA damage by quartz in alveolar epithelial cells. *Mutat. Res* **517**, 77–86.

Shtraichman, O., Blanc, P. D., Ollech, J. E., Fridel, L., Fuks, L., Fireman, E., and Kramer, M. R. (2015). Outbreak of autoimmune disease in silicosis linked to artificial stone. *Occup. Med. (Lond)* **65**, 444–450. 10.1093/occmed/kqv073.

Steenland, K., and Ward, E. (2014). Silica: a lung carcinogen. *CA Cancer J. Clin.* **64**, 63–69. 10.3322/caac.21214.

Tanjore, H., Xu, X. C., Polosukhin, V. V., Degryse, A. L., Li, B., Han, W., Sherrill, T. P., Plieth, D., Neilson, E. G., Blackwell, T. S., and., *et al.* (2009). Contribution of epithelial-derived fibroblasts to bleomycin-induced lung fibrosis. *Am. J. Respir. Crit. Care Med.* **180**, 657–665. 10.1164/rccm.200903-0322OC.

Thiery, J. P., Acloque, H., Huang, R. Y., and Nieto, M. A. (2009). Epithelial-mesenchymal transitions in development and disease. *Cell* **139**, 871–890, 10.1016/j. cell.2009.11.007.

Tomatis, M., Prandi, L., Bodoardo, S., and Fubini, B. (2002). Loss of surface reactivity upon heating amphibole asbestos. *Langmuir* **18**, 4345–4350. 10.1021/la011609w.

Vallyathan, V., Kang, J. H., Van Dyke, K., Dalal, N. S., and Castranova, V. (1991). Response of alveolar macrophages to

in vitro exposure to freshly fractured versus aged silica dust: the ability of Prosil 28, an organosilane material, to coat silica and reduce its biological reactivity. *J. Toxicol. Environ. Health* **33**, 303–315. 10.1080/15287399109531529.

Vallyathan, V., Shi, X. L., Dalal, N. S., Irr, W., and Castranova, V. (1988). Generation of free radicals from freshly fractured silica dust. Potential role in acute silica-induced lung injury. *Am. Rev. Respir. Di.S* **138**, 1213–1219. 10.1164/ajrccm/138.5.1213.

Wang, X., Xu, D., Liao, Y., Zhong, S., Song, H., Sun, B., Zhou, B. P., Deng, J., and Han, B. (2015). Epithelial neoplasia coincides with exacerbated injury and fibrotic response in the lungs of Gprc5a-knockout mice following silica exposure. *Oncotarget* **6**, 39578–39593. 10.18632/oncotarget.5532.

Yilmaz, M., and Christofori, G. (2009). EMT, the cytoskeleton, and cancer cell invasion. *Cancer Metastasis Rev*. **28**, 15–33. 10.1007/s10555-008-9169-0.